Nonlinear Ballooning Modes in Tokamaks: Stability and Saturation

C J Ham¹, S C Cowley^{1,2}, G Brochard^{1,3}, and H R Wilson^{1,4}

¹CCFE, Culham Science Centre, Abingdon, Oxon, OX14 3DB

²Rudolf Peierls Centre for Theoretical Physics, University of Oxford, Oxford OX1 3NP, UK

³Department of Physics, Imperial College, Prince Consort Road, London SW7 2BZ UK

⁴York Plasma Institute, Department of Physics, University of York, Heslington, York YO10 5DD UK

E-mail: christopher.ham@ukaea.uk

Abstract. The nonlinear dynamics of magneto-hydrodynamic ballooning mode perturbations is conjectured to be characterised by the motion of isolated elliptical flux tubes. The theory of stability, dynamics and saturation of such tubes in tokamaks is developed using a generalised Archimedes' principle. The equation of motion for a tube moving against a drag force in a general axisymmetric equilibrium is derived and then applied to a simplified 's-\alpha' equilibrium. The perturbed nonlinear tube equilibrium (saturated) states are investigated in an 's-a' equilibrium with specific pressure and magnetic shear profiles. The energy of these nonlinear (ballooning) saturated states is calculated. In some cases, particularly at low magnetic shear, these finitely displaced states can have a lower energy than the equilibrium state even if the profile is linearly stable to ballooning modes (infinitesimal tube displacements) at all radii. Thus nonlinear ballooning modes can be metastable. The amplitude of the saturated tube displacement in such cases can be as large as the pressure gradient scale length. We conjecture that triggering a transition into these filamentary states can lead to hard instability limits. A short survey of different pressure profiles is presented to illustrate the variety of behaviour of perturbed elliptical flux tubes.

1. Introduction

Ballooning modes are pressure driven instabilities that occur in magnetically confined fusion plasmas and are localized to the bad curvature region [1]. These instabilities can produce both *hard* and *soft* stability limits on the plasma. A *soft* limit is where the plasma pressure gradient is held at a critical value. If the profile goes above this value at any given point the instability is triggered and it produces sufficient transport to drive the pressure profile back to the soft limit value [2]. This may be the process that limits the pressure gradient in the pedestal region of a tokamak plasma. However, there are also *hard* limits which are characterised by an explosive loss of a significant amount of plasma energy. Examples of this are Edge Localized Modes (ELMs) [3,4], certain types

of plasma disruptions in tokamaks especially discharges with internal transport barriers (ITBs) [5] or, the core density collapse in the LHD stellarator [6]. In some cases, *e.g.* ITB disruptions, explosive instability caused by a hard limit terminates the plasma. In other cases, *e.g.* ELMs, the loss of energy takes the plasma pressure gradient well below the critical value. The plasma then reheats slowly returning the pressure gradient to the critical state thereby triggering repeated explosive events. An improved understanding of what causes a hard limit could lead to strategies to avoid it and thus confidence to run plasmas with steep pressure profiles such as tokamak plasmas with ITBs which could improve the economics of fusion power.

In a series of papers we have shown that the early nonlinear stage of the ballooning mode generates explosively unstable elliptical flux tubes – "filaments" [7, 8, 11]. The interaction between filaments (flux tubes) tends to suppress the weaker filaments leading to isolated filaments [12, 13]. Thus we have conjectured that the fully nonlinear state of the ballooning type modes is isolated displaced elliptical flux tubes [11]. This conjecture is consistent with observations of (see for example [4–6]). Some progress was made by Zhu et. al. [9, 10] in describing the transition to a fully nonlinear state. Recently we investigated the nonlinear states of an elliptical ballooning flux tube in tokamak geometry [14]. In particular, we derived a generalised *Archimedes' principle* [11] and stated the resulting nonlinear equation in toroidal geometry [14]. We will give the full details of the calculation and also survey more of the parameter space in this paper.

In [14] we found that there were ballooning flux tubes which were stable to infinitesimal perturbations but unstable to finite amplitude perturbations. In other words the flux tubes were metastable. Metastability is ubiquitous in the physical sciences but it is largely unexplored in magnetically confined fusion plasmas. For a hard instability limit to be possible a finite displaced lower energy state of the plasma must be accessible. In this paper (and in [14]) we examine the possible end states of the ballooning flux tube perturbation – specifically the equilibrium states of the flux tube. In the metastable cases we indeed find lower energy finitely displaced flux tube equilibria. When a metastable plasma approaches the linear stability boundary the energy needed to trigger the nonlinear instability tends to zero. Small amplitude noise in the plasma can trigger onset of the nonlinear instability close to the linear instability boundary. We conjecture that the ballooning mode provides a hard instability limit only if there are metastable flux tubes.

In Section 2 we give details of the derivation of the generalised *Archimedes' principle* in axisymmetric geometry. In Section 3 we calculate the required quantities for the governing equation for a simplified ' $s - \alpha$ ' type equilibrium [15]. Section 4 gives the energy change which results from the flux tube erupting. We discuss the results of a numerical investigation with given pressure gradient and magnetic shear profiles in Section 5. Discussion and Conclusions are given in Section 6. In Appendix A we discuss the conditions under which the perturbation of the field outside the elliptical tube can be ignored. The details of our simplified equilibrium calculations are given in Appendix B. Finally in Appendix C we calculate the weakly nonlinear evolution of an elliptical

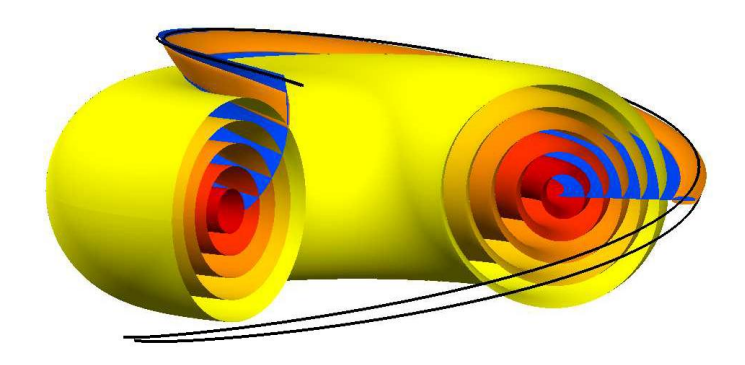


Figure 1: An elliptical (orange) flux tube sliding along the (blue) surface $S = S_0$. The external (black) field lines are only slightly perturbed. The tube crosses the (yellow) unperturbed flux surfaces labelled by the variable r. The equations for a field line in the tube which starts on the $r = r_0$ surface is $r = r(r_0, \theta, t)$ and $S = S_0$.

flux tube in the 's- α ' model.

2. Erupting flux tubes in a general axisymmetric equilibrium

In this Section we generalize the treatment of [11] to the geometry of a single isolated flux tube in a general axisymmetric stationary magnetic equilibrium. We shall assume that the flux tube is moving somewhat slower than the sound speed, since we are interested in the behaviour near marginal stability and the saturated states of the flux tube. Consider a field aligned tube of plasma that is displaced through the plasma – sliding along a surface that is parallel to the undisplaced magnetic field lines outside the tube see Figure 1. The field inside the tube is denoted B_{in} and the field outside B_{out} . The tube has an elliptical cross section, elongated in the direction of motion and narrower across $(\delta_1 \ll \delta_2)$, see Fig. 2. The exact cross sectional shape of the tube is not important here - just that it is narrow enough that the perturbation of the surrounding field is unimportant and that it is considerably elongated in the direction of motion (see discussion in Appendix A and [11]).

As the erupting tube moves it must follow a surface S, which is tangent to both the tube ($B_{in} \cdot \nabla S = 0$) and the surrounding field lines ($B_{out} \cdot \nabla S = 0$ see Figure 1). We shall assume that the surrounding field is largely unperturbed – *i.e.* $B_{out} = B_0$. We can therefore take the surface S to be a surface of a Clebsch potential of the unperturbed field, i.e $B_0 = \nabla \psi \times \nabla S$. We will use the straight line flux coordinates introduced in Greene, Johnson and Weimer [16]. Thus we use r to label flux surfaces, φ the toroidal

4

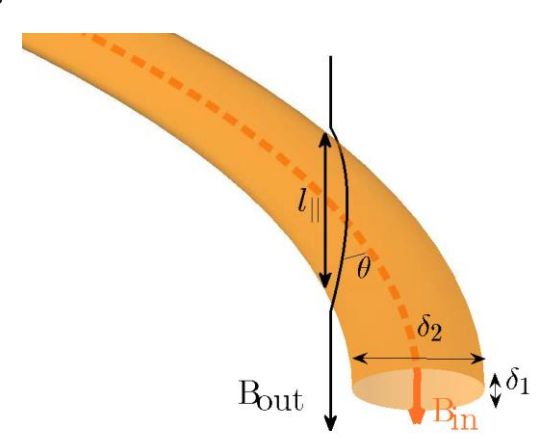


Figure 2: The filament is assumed to be elliptical in shape of width δ_1 in the direction perpendicular the surface S and δ_2 in the direction of motion along S with $\delta_2 >> \delta_1$. The external field B_{out} bends around the filament – this perturbation is discussed in Appendix A. The field just inside and just out the filament are at a finite angle θ to each other – *i.e.* $B_{in} \cdot B_{out} \sim B_{in} \cdot B_0 = B_{in}B_0 \cos \theta$. Thus there are current sheets along the sides of the filament. The fact that the flux tube is elliptical is an assumption, however this is motivated by previous work and physical intuition. First, in linear theory, [1], the eigenfunction across the field is elliptical ($\delta_1 \sim \frac{R_0}{n}, \delta_2 \sim \frac{R_0}{n}$ with $n \gg 1$). Secondly, the weakly nonlinear theory shows that the linear eigenfunction evolves into a narrow elliptical flux tube [7, 8]. Finally, the elliptical shape minimizes sideways distortion of the external field (See Appendix A.) to more efficiently extract energy in the fully nonlinear motion.

angle and, θ the straight field-line poloidal angle. We deviate slightly from [16] in choosing $\theta = 0$ to be the outer midplane rather than inner midplane for the simplified circular flux surface ('s - α ') equilibrium of our example. In the notation of [16]:

$$\mathbf{B}_0 = -\bar{\mathbf{B}}_0 R_0 f(r) \nabla r \times \nabla \mathbf{S} \text{ where } \mathbf{S} = \varphi - q(r) (\theta - \theta_0(r)). \tag{1}$$

Where \vec{B}_0 and R_0 are constants, q(r) is the safety factor and $\theta_0(r)$ is an arbitrary function. The trajectory of a field line in the flux tube that is displaced from the surface r_0 is:

$$r = r(\theta, r_0, t),$$
 and $S = constant$ (2)

with the boundary condition $r \to r_0$ as $|\theta| \to \infty$. Note θ measures position along the field line.

The choice of Clebsch potentials is not unique. In principle, we could consider motion along any S surface defined by any function $\theta_0(r)$. In the 's - α ' examples given here we restrict ourselves to the choice $\theta_0(r) = 0$. This is the choice for the most linearly unstable motions but not necessarily the most nonlinearly unstable. It is not *a priori* obvious how to choose S, the Clebsch surface. Indeed it is likely to be determined by the

dynamics (i.e. the flux tube defines the Clebsch surface S as it erupts) and outside our considerations here. Our general theory applies to cases where $\theta_0(r) \neq 0$ but we have not explored any specific such cases. The tube wraps around the torus many times and we consider $r(\theta, r_0, t)$ on the domain $-\infty < \theta < \infty$. We ignore the fact that the S surface intersects itself as θ increases since we assume that the perturbations are sufficiently localised in θ to avoid self intersection of the flux tube. Note this assumption can hold even when the tube localisation in θ is much greater than 2π (as long as r_0 is not a low order rational surface e.g. $q(r_0) = 1$). We also assume that flux tubes do not intersect other displaced tubes. The plasma is taken to be perfectly conducting -i.e. the plasma is frozen to the field. Thus the field lines must remain attached to their original surfaces and therefore $r = r(\theta, r_0, t) \rightarrow r_0$ as $|\theta| \rightarrow \infty$. Clearly the surface S twists, the local twist is a measure of the *local shear* – note the twist of the blue surface in Figure 1. The twist stretches the flux tube making it narrower and longer (Figure 1) as $|\theta|$ increases.

We define the perpendicular vector that is also tangent to the S surface

$$\mathbf{e}_{\perp} = \frac{1}{B_0} \nabla \mathbf{S} \times \mathbf{B}_{0},\tag{3}$$

We define three equilibrium quantities
$$u_{\mathbb{I}} = u_{\mathbb{I}}(r,\theta) = -\bar{B}_{0}R_{0}f\frac{1}{B_{0}}B_{0} \cdot \nabla\theta,$$

$$u_{\perp} = u_{\perp}(r,\theta) = \bar{B}_{0}R_{0}f\frac{1}{B_{0}}e_{\perp} \cdot \nabla\theta, \quad w^{2} = w^{2}(r,\theta) = \frac{u^{2}|e_{\perp}|_{\mathbb{I}}^{2}}{B_{0}^{2}}.$$

$$(4)$$

Where $|B_0| = B_0$ (not to be confused with the constant \bar{B}_0). Since $B_{in} \cdot \nabla S = 0$ we must be able to write

$$B_{in} = B_{II}(\theta, r_0, t)B_0 + B_{\perp}(\theta, r_0, t)e_{\perp}$$
 (5)

The equation for a field line inside the tube is:

$$\frac{O_{r}}{\partial \theta} \Big|_{r_{0},t} = \frac{B_{in} \cdot \nabla r}{B_{in} \cdot \nabla \theta} = \frac{B_{\perp}}{B_{\perp} u_{\perp} - B_{\perp} u_{\perp}} \tag{6}$$

The force (per unit volume) on the plasma is:

$$\mathbf{F} = -\frac{1}{\mu_0} \nabla \frac{B^2}{2} + \mu_0 p + \frac{1}{\mu_0} \mathbf{B} \cdot \nabla \mathbf{B}. \tag{7}$$

The force across the narrow tube (in the ∇S direction) is formally large, $O(p/\delta_1)$, and must cancel to this order, i.e.

From Sider, i.e.
$$F \cdot \nabla S \sim -\frac{1}{\mu_0} |\nabla S|^2 \frac{\partial}{\partial S} \left(\mu_0 p + \frac{B^2}{2} \right) = 0 \tag{8}$$

Thus integrating across the tube we get:

$$\mu_0 p_{in} + \frac{B_{in}^2}{2} = \mu_0 p_{out} + \frac{B_{out}^2}{2}$$
 (9)

where 'in' refers to inside the tube and 'out' refers to just outside the tube (at the same r and θ along the tube). We will assume that the field and pressure outside the tube are unperturbed (this sets a condition on δ_1 and δ_2 See Appendix A.) so that:

$$p_{out} = p_0(r)$$
 and $B_{out} = B_0(r, \theta)$ (10)

are known. The total pressure forces at a point on the tube are thus identical to the pressure forces on the plasma it replaced. We shall assume that the motion of the tube is slow enough that pressure balance along the tube is established -i.e. $p_{in} = p(r_0)$. This approximation is obviously correct in the stationary end state of the eruption -a lower energy equilibrium with a finitely displaced tube. Thus

$$B_{in}^2 = B_0^2 + 2\mu_0(p(r) - p(r_0)) \tag{11}$$

Using equation (5) we obtain:

$$B_{\text{II}}^{2} = 1 + \frac{2\mu_{0}(p(r) - p(r_{0}))}{B_{0}^{2}} - B_{1}^{2} \frac{|\mathbf{e}_{\perp}|^{2}}{B_{0}^{2}}$$
(12)

Thus we obtain expressions for $B_{\rm II}$ and B_{\perp}

$$B_{\mathrm{II}} = \left\{ \begin{vmatrix} \frac{1 + \frac{2\mu_{0}(p(r) - p(r_{0}))}{B_{0}^{2}} & \mathbf{i} \\ \frac{(\partial r)}{B_{0}^{2}} & 1 + u_{\perp} & \frac{\partial r}{\partial \theta} \\ 1 + u_{\perp} & \frac{\partial \theta}{\partial \theta} & r_{0} & + w^{2} \frac{\partial \theta}{\partial \theta} & r_{0} \end{vmatrix} \right\} + u_{\perp} = \left\{ \frac{\partial r}{\partial \theta} \right\}_{r_{0}}^{\#}$$

$$B_{\perp} = \left\{ \begin{array}{c} \frac{1 + \frac{2\mu_0(p(r) - p(r_0))}{Bb}}{1 + \mu_{\perp} \frac{(\partial r)}{\partial \theta} r_0} & \mathbf{i} \\ \frac{1}{1 + \mu_{\perp} \frac{(\partial r)}{\partial \theta} r_0} & \mathbf{i} \\ \frac{\partial r}{\partial \theta} & \mathbf{i} \\ \frac{\partial r}{\partial \theta} & \mathbf{i} \\ \end{array} \right\} \begin{pmatrix} \# \\ \mathbf{i} \\ \mathbf{i}$$

Substituting $r = r(\theta, r_0, t)$ into p(r), $B^2(r, \theta)$, $u_{\perp}(r, \theta)$, $u_{II}(r, \theta)$ and $w^2(r, \theta)$ in these expressions yields $B_{II}(\theta, r_0, t)$ and $B_{\perp}(\theta, r_0, t) - i.e.$ along the field line labelled by r_0 .

The ideal MHD force, F_{\perp} pushing the field line along S in the direction $\mathbf{e}_{\perp} = (\nabla \mathbf{S} \times \mathbf{B}_0)/B_0$ is:

$$F_{\perp} = \mathbf{F} \cdot \mathbf{e}_{\perp} = 1 \frac{1}{\mu_{0}} \mathbf{B}_{in} \cdot \nabla \mathbf{B}_{in} - \nabla \frac{\mathbf{B}_{in}^{2}}{2} + \mu_{0} p_{in} \cdot \mathbf{e}_{\perp}$$

$$= \frac{1}{\mu_{0}} [\mathbf{B}_{in} \cdot \nabla \mathbf{B}_{in} - \mathbf{B}_{0} \cdot \nabla \mathbf{B}_{0}] \cdot \mathbf{e}_{\perp}.$$
(14)

The second expression follows from Eq. (9) and the unperturbed equilibrium relation $\nabla (B_0^2/2 + \mu_0 p_0) = B_0 \cdot \nabla B_0$. Eq. (14) is valid when the tube is sufficiently elliptical that $\delta_1^2 R_0 \sin^2 \theta \ll \delta_2^3$ where θ is the angle betwee B_{in} and B_{out} – see Appendix A. The expression in Eq. (14) is a generalised form of *Archimedes' principle* where the net force is the curvature force of the tube minus the curvature force of the tube it has displaced.

Substituting equation (5) into (14) we obtain
$$\mu_{0}F_{\perp} = (B_{\parallel} - 1)(B_{0} \cdot \nabla B_{0}) \cdot e_{\perp} + B_{0}(B_{\Pi}B_{0} + B_{\perp}e_{\perp}) \cdot \nabla \frac{|e_{\perp}|^{2}B_{\perp}}{B_{0}}$$

$$-B_{\perp}^{2}B_{0}^{2}e_{\perp} \cdot \nabla \frac{|e_{\perp}|^{2}}{2B_{0}^{2}}.$$
(15)

Equation (15) with B_{II} and B_{\perp} given by equation (13) determines the force given the shape of the field line, $r(\theta, \psi_0)$ for each r_0 . Note that by definition $B_{in} \cdot \nabla r_0 = (B_{II}B_0 + B_{\perp}e_{\perp}) \cdot \nabla r_0 = 0$ and therefore $B_{in} \cdot \nabla \equiv B_{in} \cdot \nabla \theta \begin{pmatrix} 0 \\ 0 \end{pmatrix}$ Therefore we can treat

 r_0 as a parameter in equation (15). For an infinitesimal perturbation $(r - r_0 = \xi \ll r_0)$ equation (15) reduces to the form familiar from the linear ballooning equation of Connor *et al.* [1]

$$\frac{-\mu_0}{\bar{B}_0 R_0 f} F_{\perp} \sim B_0 B_0 \cdot \nabla \frac{\left(|\mathbf{e}_{\perp}|^2 - \mathbf{B}_0^2 - \mathbf{E}_0^2\right)}{B_0^2} B_0 \cdot \nabla \xi + \frac{2\mu_0}{B_0^3} (\mathbf{e}_{\perp} \cdot \nabla p) \mathbf{e}_{\perp} \cdot (\mathbf{B}_0 \cdot \nabla \mathbf{B}_0) \xi. (16)$$

The first term in this equation arises from the extra line bending of field lines by the perturbation and is stabilizing. The second term is the change of the field line bending force due to the change of field strength (sometimes called the interchange drive)

The flux tube can have several equilibrium states. Obviously the unperturbed state $r = r_0$, $B_{\perp} = 0$ and $B_{\text{II}} = 1$ is an equilibrium. We are interested in finding displaced equilibria. Such states of the flux tube must satisfy $F_{\perp} = 0$ which we write as:

$$(B_{\mathbb{I}}u_{\mathbb{I}} - B_{\perp}u_{\perp}) \frac{\partial B_{\perp}}{\partial \theta} \Big|_{r_0} = (B_{\mathbb{I}}^2 - 1)a_1 + B_{\perp}B_{\mathbb{I}}a_2 + B_{\perp}^2 a_3$$
 (17)

where u_{\perp} and $u_{\rm II}$ are defined in equation (4) the coefficients are

$$a_{1} = a (r, \theta) = \frac{\bar{B}_{0} R_{0} f e_{\perp} \cdot (B_{0} \cdot \nabla B_{0})}{|e_{\perp}|^{2} B_{0}}$$

$$a_{2} = a_{2}(r, \theta) = \frac{\bar{B}_{0} R_{0} f B_{0} \cdot \nabla (\frac{|e_{\perp}|^{2}}{B_{0}})}{|e_{\perp}|^{2}}$$

$$a_{3} = a_{3}(r, \theta) = \frac{\bar{B}_{0} R_{0} f e_{\perp} \cdot \nabla (|e_{\perp}|^{2})}{2|e_{\perp}|^{2} B_{0}}.$$
(18)

Equations (17) and (6) with $B_{\rm II}$ determined from Equation (12) constitute a second order system of one dimensional nonlinear ordinary differential equations for $r=r(\theta, r_0)$ and $B_{\perp}=B_{\perp}(\theta, r_0)-i.e.$ the equilibrium shape of the displaced field line. As before the equilibria are attained through flux frozen motion so the field lines must stay connected to their original surface. Thus we apply the boundary conditions $r \to r_0$ as $\theta \to \infty$. The tube consists of field lines from a region of r_0 — we can solve for each field line independently since r_0 is merely a parameter in equation (17). However the calculation of the cross sectional shape of the tube is beyond the scope of this paper — see Appendix A.

3. Nonlinear Ballooning Equation in simplified toroidal geometry

We next simplify the nonlinear ballooning equation in general geometry to the large aspect ratio equilibrium with a transport barrier. We calculate the required metrics in a large aspect ratio toroidal geometry with two regions, an outer region where the pressure gradient is small and an narrow (of width $\Delta r \sim O(\rho)$) inner region where the pressure gradient is large, so that we can obtain the nonlinear ballooning equation for this case. We calculate all the elements of the force equation to find a nonlinear generalisation of the ' $s - \alpha$ ' ballooning equation. We need the metric elements from

the ' $s - \alpha$ ' large aspect ratio equilibrium. The details of the equilibrium are given in Appendix B.

Using $S = \varphi - q(r)(\theta - \theta_0)$ and metric coefficients from Appendix A.

$$|\mathbf{e}_{\perp}|^2 = |\nabla \mathbf{S}|^2 = \frac{q^2}{r^2} \left[1 + (s(\theta - \theta_0) - \alpha \sin \theta)^2) + O(q).... \right]$$
 (19)

where s = rq'/q is the magnetic shear and $\alpha = -2\mu_0 R_0 p' q^2 / \bar{B}_0^2$ is the normalised pressure gradient. We have taken $\theta_0 = \text{constant}$ since for this simple case we expect that $\theta_0 = 0$. In general we can consider cases with θ_0 a function of r. Using the metric coefficients from the Appendix we obtain:

$$u_{\perp} = \frac{s(\theta - \theta_0)}{r} + O(\frac{\varrho}{r}).... \tag{20}$$

$$u_{II} = -\frac{\bar{B}_0 r}{q^2 R_0} + O(\bar{B}_0 q^2).....$$
 (21)

$$w^{2} = \frac{1}{q^{2}R_{0}^{2}} \left[1 + (s(\theta - \theta_{0}) - \alpha \sin \theta)^{2}) + O(\varrho).... \right]$$
 (22)

The magnetic curvature can be expressed as

$$(\mathbf{B}_0 \cdot \nabla \mathbf{B}_0) \cdot \mathbf{e}_{\perp} = \mathbf{e}_{\perp} \cdot \nabla \qquad \frac{\mathbf{B}_0^2}{2} + p_0(r)$$

$$= \frac{q\bar{B}^2}{rR_0} \left[\cos\theta + \sin\theta(s(\theta - \theta_0) - \alpha\sin\theta)\right]$$
 (23)

The displacement of the flux tube is taken to be of order the transport barrier width so that

$$r - r_0 \sim O(r\varrho) \rightarrow \frac{Q_T}{\partial \theta} \sim O(r\varrho)$$
 (24)

which allows the following simplifications

$$B_{\mathbb{I}}^{2} - 1 = \frac{2\mu_{0}(p_{2}(r) - p_{2}(r_{0}))}{I_{0}^{2}} \sim O(\rho^{2})$$
 (25)

and

$$B_{\perp} = -\frac{\bar{B}_0 r}{q^2 R^0} \left(\frac{\partial r}{\partial \theta} \right) \sim O(\bar{B}_0 r \varrho^2)$$
 (26)

$$(\mathbf{B}_{in} \cdot \nabla \theta) = \frac{\bar{B}_0}{qR_0} + O(\frac{B_0 \varrho}{qR_0}) \tag{27}$$

We have now calculated all of the elements required for the nonlinear ballooning Eq. (14). Substituting them into Eq. (14) gives the nonlinear ballooning operator in a large aspect ratio tokamak with a transport barrier

$$-F_{\perp} \frac{\mu_0 q R^2 r}{\bar{B}_0^2} = (\beta_N(r_0) - \beta_N(r)) \left[\cos \theta + \sin \theta (s\theta - \alpha \sin \theta)\right]$$

$$+\frac{\partial}{\partial \theta} \left[1 + (\alpha \sin \theta - s\theta)^{2}\right] \frac{\partial r}{\partial \theta} - \frac{1}{r_{0}} \frac{\partial r}{\partial \theta} - \frac{1}{r_{0}} \frac{\partial r}{\partial \theta} \frac{\partial r}{\partial \theta} - \frac{1}{r_{0}} \frac{\partial r}{\partial \theta} \frac{\partial r}{\partial \theta} - \frac{1}{r_{0}} \frac{\partial r}{\partial \theta} \frac{\partial r}{\partial \theta} \frac{\partial r}{\partial \theta} - \frac{1}{r_{0}} \frac{\partial r}{\partial \theta} - \frac{1}{r_{0}}$$

where

$$\beta_N(r) = 2R q^2 \frac{\mu_0 p_2(r)}{\bar{I}_0^2} \rightarrow \alpha(r) = -\frac{d\beta_N(r)}{dr}$$
 (29)

Our notation for $\beta_N(r)$ is deliberately reminiscent of the normalised beta of Troyon [21], however our variable is not normalised in quite the same way as Troyon's. Note that in Eq. (28) α is a function of r so that:

$$\frac{\partial \alpha}{\partial \theta} = \frac{\partial r}{\partial \theta} = \frac{\partial r}{\partial \theta} = \frac{\partial \alpha}{\partial r} = \frac{\partial \alpha}{\partial r}$$
(30)

Our current equation only gives the force. This will allow us to find the saturated states, $F_{\perp} = 0$, but it does not allow us to look at the time dependent solution of the system. If we assume the time evolution is dominated by viscous drag we can develop a time dependent evolution equation. This is probably too simplistic but it does however allow us the examine the energy evolution. We first need an expression for the velocity, $v = ve_{\perp}$ so that

$$\mathbf{v} \cdot \nabla r = \frac{\partial r}{\partial t} \quad \rightarrow \quad \mathbf{v} = -R \int_{0}^{\mathbf{r}} \frac{\partial r}{\partial t} = -\frac{r \partial r}{q \partial t}$$
(31)

where we have used $f = \frac{r}{Roq} + O(q^2)$. We introduce a drag to balance the force $F_{\perp} = vv \cdot e_{\perp}$ (similar to [11]) so that:

$$v' \frac{\partial r}{\partial t} \left[1 + (\alpha \sin \theta - s\theta)^2 \right] =$$

 $(\beta_N(r_0) - \beta_N(r)) [\cos \theta + \sin \theta (s\theta - \alpha \sin \theta)]$

$$+\frac{\partial}{\partial \theta} \left[1 + (\alpha \sin \theta - s\theta)^{2}\right] \frac{\partial r}{\partial \theta} - \frac{1}{r_{0}} \frac{\partial r}{\partial \theta} - \frac{1}{r_{0}} \frac{\partial r}{\partial \theta} \frac{\partial r}{\partial \theta} - \frac{1}{r_{0}} \frac{\partial r}{\partial \theta} \frac{\partial r}{\partial \theta} - \frac{\partial r}{\partial \theta} \frac{\partial r}{\partial \theta} - \frac{\partial r}{\partial \theta} \frac{\partial r}{\partial \theta} - \frac{\partial r}{\partial \theta} \frac{\partial r}{\partial \theta}$$
(32)

with $v' = v \frac{\mu_0 q^2 R_0}{B_0^2}$. This a nonlinear evolution equation for the flux tube position $r(\theta, r_0, t)$. Note that if we linearise Eq. (32) $(r - r_0 \ll \rho r)$ we recover the usual ' $s - \alpha$ ' equation for ballooning modes.

Figure 1 shows a typical solution of the ballooning mode equation in simplified toroidal geometry. A orange flux tube has ballooned out, moving along the blue surface S=0. This surface is twisted because of the magnetic shear in the system. The flux tube parts the black field lines outside which means that the flux tube can move without

reconnection ocuring. The displacement of the flux tube is larger on the low field, or outboard, side. The flux tube is stretched on the inboard side due to the magnetic shear. In figure 1 the trajectory (in θ) of the displaced field lines inside the tube is a solution of the ballooning equation (32) and the distortion of the cross section by magnetic shear is calculated – however the outboard shape of the tubes is guessed.

4. Energy Equation

In [11] we derived an energy (or action) functional $E = E[r(\theta, r_0), r_0]$ that is stationary

for equilibria and minimised for stable equilibria. This is;
$$E = \int_{-\infty}^{\infty} B_{in} \cdot d\mathbf{r} = \int_{-\infty}^{\infty} B^{2}_{in} \frac{d\theta}{B_{in} \cdot \nabla \theta}$$

$$= Z_{\infty} \int_{-\infty}^{\infty} \mathbf{S} \frac{1}{1 + u_{\perp}} \frac{\partial r}{\partial \theta} \int_{r_{0}}^{-2} \mathbf{R} \frac{\partial r}{\partial \theta} \int_{r_{0}}^{2} \mathbf{R} d\theta$$

where we have used Eq. (22). This integral is performed keeping r_0 constant -i.e.we take $r = r(\theta, r_0, t)$. The integral is formally infinite so we should subtract the unperturbed integral – Eq. (33) with $r = r_0$.

Expanding in inverse aspect ratio for our case we obtain the energy/action functional:

$$E = \frac{Z_{\infty} \int_{-\infty}^{\infty} \frac{1}{1} \left(\frac{1}{\partial r} \right)_{2}^{2} \left(1 + (\alpha \sin \theta - s\theta)^{2} \right)^{\#}$$

$$- \frac{Z_{\infty}}{1} \int_{-\infty}^{\infty} \frac{1}{2} \frac{1}{\partial \theta} \int_{r_{0}}^{r_{0}} \left(A(r, r) \cos \theta + B(r, r) \theta \sin \theta - C(r, r) (\sin \theta)^{2} \right)^{2}$$
(33)

where the new coefficients are:

We coefficients are:

$$Z_{r}$$

$$A(r, r_{0}) = (\beta_{N}(r_{0}) - \beta_{N}(r'))dr'$$

$$Z_{r}$$

$$B(r, r_{0}) = (\beta_{N}(r_{0}) - \beta_{N}(r'))s(r')dr'$$

$$C(r, r) = (\beta_{N}(r_{0}) - \beta_{N}(r'))^{2}$$

$$C(r, r) = (\beta_{N}(r_{0}) - \beta_{N}(r))^{2}$$

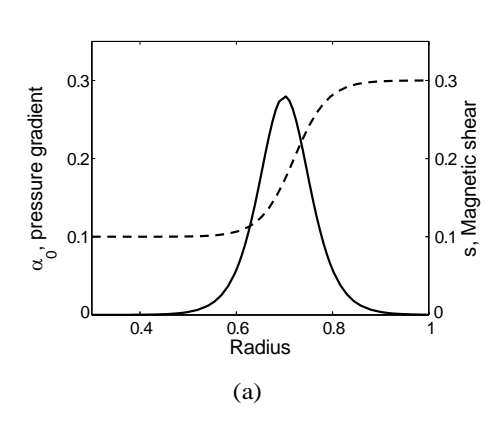
$$C(r, r) = (\beta_{N}(r_{0}) - \beta_{N}(r)$$

$$C(r, r) = (\beta_{N}(r_{0}) - \beta_{N}($$

It is straight forward to show that equilibrium solutions of equation (32) $(F_{\perp} = 0)$ are stationary states ($\delta E = 0$)under variation of $r = r(\theta, r_0)$ in (33). The evolution of E using Eq. (32) is

$$\sum_{r=0}^{1} \frac{\mathbf{i}}{r} \left(\frac{\partial r}{\partial t} \right)_{r_{0},\theta} \left(1 + (\alpha \sin \theta - s\theta)^{2} \right)^{\#} = -\frac{d\mathbf{E}}{dt}.$$
(35)

Note that the energy must always decrease in the drag evolution so that it seeks out the minimum energy equilibrium states.



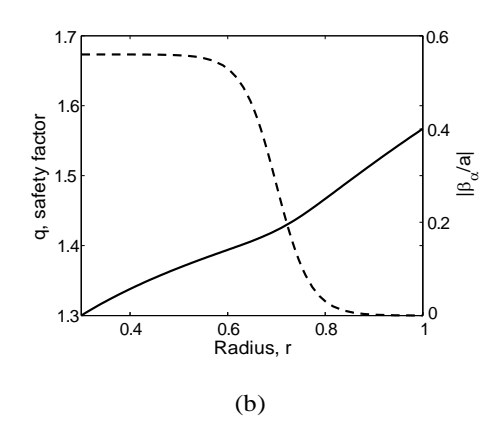


Figure 3: Transport barrier profiles used in the numerical investigation: a) magnetic shear, s(r), and pressure gradient $\alpha(r)$; and b) safety factor and pressure profiles used for this numerical investigation. The parameters for this case are: $s_0 = 0.1$, $s_1 = 0.3$, $\alpha_0 = 0.28$, q = 0.07, $r_a = 0.7$ and $r_s = 0.72$ see equations (36) and (37).

5. Numerical investigation

The nonlinear 's - α ' equation derived in the previous section is solved numerically in this section. We focus on calculating the saturated states from $F_{\perp} = 0$ where F_{\perp} is given in equation (28). A time dependent method (Solution of equation (32)) was used in [14].

5.1. Profiles

We investigate the model of a transport barrier type of equilibrium, since we see filamentary structures exploding from such profiles in tokamak experiments, for example, ELMs from the edge transport barrier or ballooning modes from ITBs in TFTR [5]. The model is specified in terms of magnetic shear s(r), and pressure gradient, $\alpha(r)$. The pressure gradient for this model is

model is specified in terms of magnetic shear
$$s(r)$$
, and pressure gradient, $\alpha(r)$. The pressure gradient for this model is
$$\alpha = -\frac{d\beta_N}{dr} = \alpha \operatorname{sech}^2 \frac{r - r_\alpha}{\varrho}.$$
(36)

and the shear profile is

profile is
$$s(r) = s_0 + \frac{s_1 - s_0}{2} \tanh \frac{r - r_s}{s_0} + 1 . \tag{37}$$

These produce pressure and β profiles $p_2(r) = \varrho p_2 \quad 1 - \tanh \quad \frac{r - r_\alpha}{\varrho}$ (38)

which gives a plasma
$$\beta_N$$
 profile
$$\beta_N(r) = \alpha_0 \rho \quad 1 - \tanh \frac{r - r_\alpha}{\rho} \quad . \tag{39}$$

For instability (linear or nonlinear) it is not sufficient that a displaced stationary (equilibrium) state is available for a flux tube, such states must be energetically favourable (i.e. E < 0) as well. We therefore need to calculate the change in energy for our profiles. The integrals in equation (34) can be calculated exactly for the profiles of pressure and shear that we are using by noting that

$$A(r, r_0) = \frac{\left(\beta_N(r') - \beta_N(r_0)\right)dr'}{r_0 \left(\left(\frac{r' - r_\alpha}{\rho}\right) - r' \tanh \frac{r_0 - r_\alpha}{\rho}\right)}$$
(40)

$$B(r_{0}) = \sum_{s=0}^{\infty} (\beta_{N}(r') - \beta_{N}(r_{0}))s(r')dr'$$

$$= \frac{s_{0} + s_{1}}{2} A(r, r) + \rho \alpha \frac{s_{1} - s_{0}}{2} \times$$

$$\begin{pmatrix} c & c & c & c \\ r' + \rho \cot & r & c & c \\ 0 & c & c & c \\ 0 & c$$

$$C(r, r_0) = \frac{1}{2} {\binom{\beta_N(r) - \beta_N(r_0)}{{\binom{\gamma_0 - r_\alpha}{2}}}} \left({\binom{\gamma_0 - r_\alpha}{\gamma_0 - \tanh}} - \tanh \frac{r_0 - r_\alpha}{\gamma_0} \right)$$

$$= \frac{q^2 q^2}{2} \tanh \frac{r_0 - r_\alpha}{\gamma_0 - \tanh}$$
(42)

5.2. Solving for stationary equilibrium states

Any elliptical flux tube is made up of a bundle field lines from differing surfaces r_0 – each can be treated separately. We find for each field line (r_0) the time independent (stationary) equilibrium states by setting the time derivatives in Eq. (32) to zero and using a shooting method. Specifically we take a long domain, $-\theta_{max} < \theta < \theta_{max}$, where $\theta_{max} \gg 1$. We solve the second order nonlinear ordinary differential equation:

$$0 = (\beta_N(r_0) - \beta_N(r)) \left[\cos\theta + \sin\theta(s\theta - \alpha\sin\theta)\right]$$

$$+\frac{d}{d\theta} \left[1 + (\alpha \sin \theta - s\theta)^{2}\right] \frac{dr}{d\theta} - \frac{1}{r_{0}} \frac{dr}{d\theta} \left[1 + (\alpha \sin \theta - s\theta)^{2}\right] \frac{dr}{d\theta} - \frac{1}{r_{0}} \frac{dr}{d\theta} \left[1 + (\alpha \sin \theta - s\theta)^{2}\right] \frac{dr}{d\theta} - \frac{1}{r_{0}} \frac{dr}{d\theta} \left[1 + (\alpha \sin \theta - s\theta)^{2}\right] \frac{dr}{d\theta} - \frac{1}{r_{0}} \frac{dr}{d\theta} \left[1 + (\alpha \sin \theta - s\theta)^{2}\right] \frac{dr}{d\theta} - \frac{1}{r_{0}} \frac{dr}{d\theta} \left[1 + (\alpha \sin \theta - s\theta)^{2}\right] \frac{dr}{d\theta} - \frac{1}{r_{0}} \frac{dr}{d\theta} \left[1 + (\alpha \sin \theta - s\theta)^{2}\right] \frac{dr}{d\theta} - \frac{1}{r_{0}} \frac{dr}{d\theta} \left[1 + (\alpha \sin \theta - s\theta)^{2}\right] \frac{dr}{d\theta} - \frac{1}{r_{0}} \frac{dr}{d\theta} -$$

for $r = r(\theta, r_0)$ with the boundary conditions $r(-\theta_{max}, r_0) = 0$ and $\frac{dr}{d\theta}$ $(-\theta_{max}, r_0) = u_{shoot}$. By varying u_{shoot} and resolving equation (43) we find the values of u_{shoot} for which $r(\theta_{max}, r_0) = 0$ – these are the stationary field line equilibrium states $r = r_{eq}(\theta, r_0)$. For each equilibrium state we calculate the energy E from equation (34) with $r = r_{eq}(\theta, r_0)$

in the coefficients given by equations (40), (41) and (42). Clearly the unperturbed state, $u_{shoot} = 0$ for which E = 0, is always an equilibrium state. For the profiles we considered we found that field lines originating from a given r_0 could be in one of four distinct categories. The first category is field lines that are both linearly and nonlinearly stable in which there is only one equilibrium state, the stable unperturbed state with E = 0see Figure (4.a). The second category is linear and nonlinearly stable field lines where there are three equilibrium states: a stable unperturbed state with E = 0, an unstable displaced equilibrium state with $E = E_1 > 0$ and, a linearly stable displaced equilibrium state with $E = E_2 > 0$ and $E_1 > E_2 > 0$ – see Figure (4.b). The third category is metastable field lines where there are three equilibrium states: a linearly stable unperturbed state with E = 0, an unstable displaced equilibrium state with $E = E_1 > 0$ and, a stable displaced equilibrium state with $E = E_2 < 0$ – see Figure (4.c). Finally the fourth category is linearly unstable field lines where there are three equilibrium states: a unstable unperturbed state with E = 0, a metastable displaced equilibrium state with $E = E_1 < 0$ and, a stable displaced equilibrium state with $E = E_2 < E_1 - see$ Figure (4d). In some profiles field lines from different r_0 are in different categories and a flux tube perturbation may contain field lines from several categories. Finding the field line equilibria is considerably faster than the time dependent method used in [14] and so we focus on it here. We have looked at the convergence with respect to the truncated domain length (i.e. θ_{max}) and we have picked a value of the θ_{max} (a typical value is $\theta_{max} = 300 \text{ radians}$) such that the results $(r = r_{eq}(\theta, r_0) \text{ and } E)$ are well converged yet the run takes a reasonable time.

5.3. First category profiles

In this section we find profiles for which all field lines (r_0) are in the first category, i.e. they have only one equilibrium state, the unperturbed state, and it is stable – see Figure (4.a). We call such profiles first category profiles. Profiles are visualised by plotting the trajectory of $s(r_0)$ and $\alpha(r_0)$ in 's – α ' space as r_0 varies from 0 to 1. In Fig. 5 and in Fig. 6 we plot eight trajectories (dashed-dotted lines) that are first category profiles. We also show the well known linear stability boundary for the ' $s-\alpha$ ' model [15]. These profiles were chosen by first fixing the values of s_0 and s_1 , which amounts to specifying the magnetic shear profile. Then we varied the pressure profile (α_0) until we found the largest possible α_0 for a first category profile with the given shear profile. Therefore profiles with larger α_0 must be in either the second third or fourth category. If there is no space between the profile trajectory and the linear stability boundary then there are no second or third category field lines (see Figures (4.b) and (4.c)) for that magnetic shear profile. A large space between the profile and the linear stability boundary means that displaced filamentary states (second or third category field lines) are available in that region. These plots therefore give an indication of the boundaries of the region in ' $s-\alpha$ ' space where nonlinear displaced states are available. However, these are not necessarily lower energy states with third category field lines (metastability).

Nonlinear ballooning 14

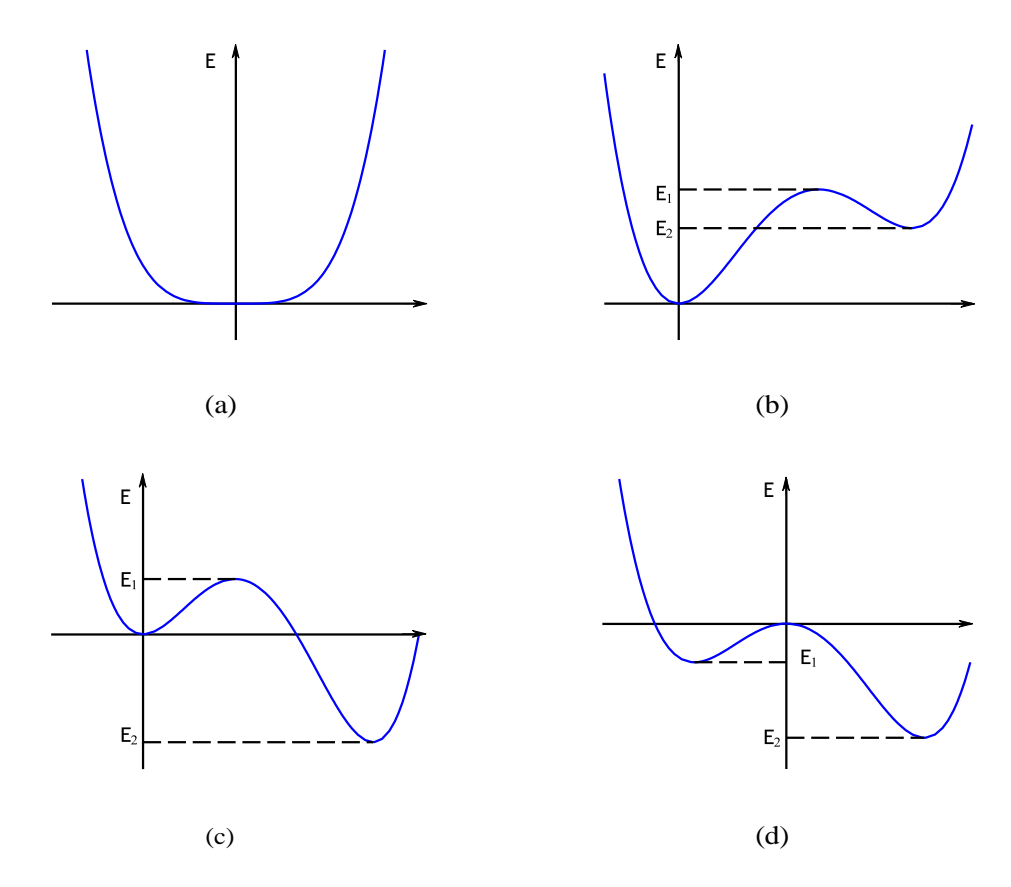


Figure 4: Schematic visualisation of field line energy surfaces for the four categories. The horizontal axes "represents" displacement – strictly speaking energy is a functional of $r(\theta, r_0)$ and therefore the energy surface is in a infinite dimensional function space not the one dimensional line plotted here. In a) (the first category) the field line is stable to linear and nonlinear perturbations. In b) (the second category) the field line is also stable to linear and nonlinear perturbations – although it would be possible for a field line to be caught in the metastable displaced state with energy E_2 . Field lines in the third category are metastable and are illustrated in c) – an energy greater than E_1 is needed to destabilise the unperturbed state. In d) the field lines are linearly unstable (category four). Drag evolution will take an arbitrary field line perturbation to an energy minimum equilibrium – see equation (35).

The results in Fig. 5 show that there are more displaced states available at lower shear.

5.4. Profiles with second and third category field lines

Next, we look at a set of profiles which are stable throughout but have regions of second and third category field lines – displaced equilibrium states. Figures 7, 8 and 9 show three such profiles. Figure 7 has the largest pressure and the profile is close to the linear stability boundary. There are displaced equilibrium field line states for a broad range $0.6 < r_0 < 0.7$ – outside this range all field lines are in the

Nonlinear ballooning 15

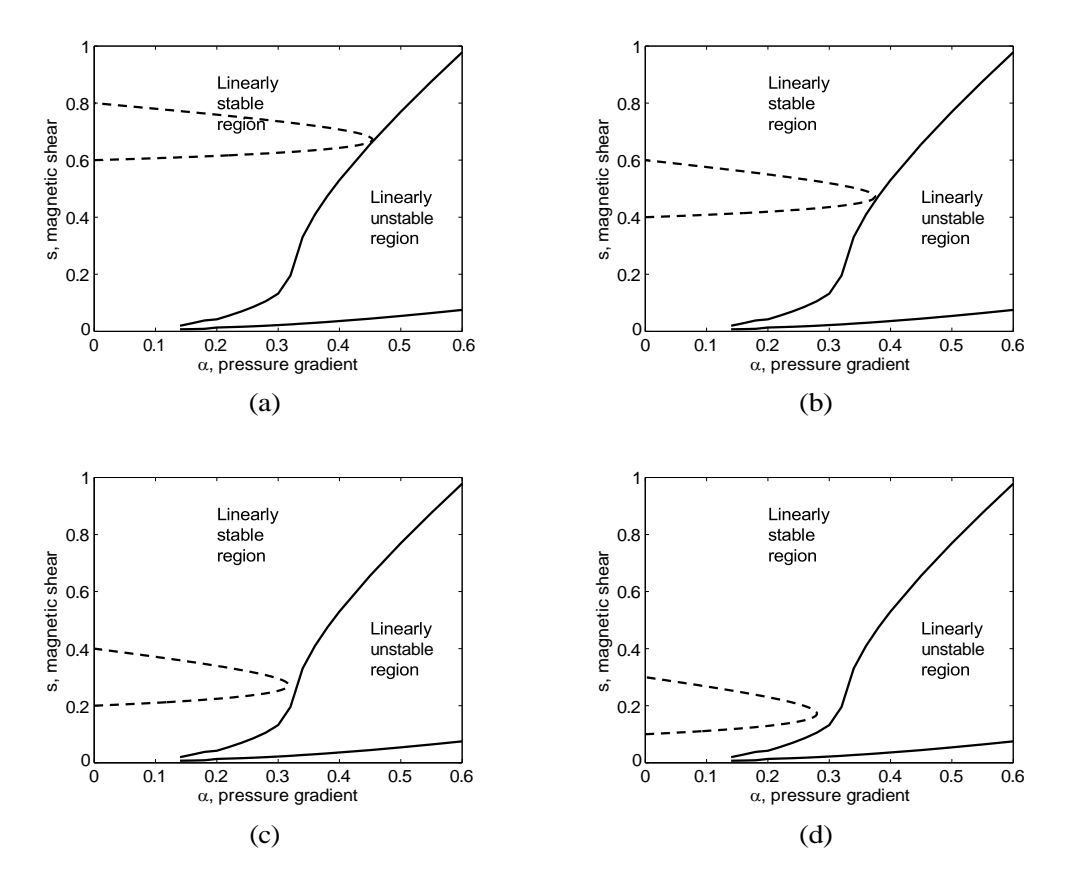


Figure 5: Trajectories (dashed-dotted lines) in the ' $s - \alpha$ ' diagram for first category profiles, see Subsection (5.3), and the linear stability boundary (solid line). The profile starts with the lower value of magnetic shear at the magnetic axis of the plasma and ends at the higher value of shear at the plasma edge. These plots are calculated by fixing the values of s_0 and s_1 and then varying α_0 to find the highest value of α_0 for a first category profile with the given shear profile. The region between the profile trajectory, dashed-dotted line, and the ballooning stability boundary, solid line, indicates the region where nonlinear displaced states are available. The values of shear profiles for each plot are: (a) $s_0 = 0.6$, $s_1 = 0.8$; (b) $s_0 = 0.4$, $s_1 = 0.6$; (c) $s_0 = 0.2$, $s_1 = 0.4$; and (d) $s_0 = 0.1$, $s_1 = 0.3$.

first category. For $0.6 < r_0 < 0.64$ the field lines are in the second category, *i.e.* $E_2 > 0$. There is also a region of third category (metastable) field lines where energy is released in a displacement from the unperturbed state to the displaced equilibrium state, $r_0 = 0.64 - 0.7$, *i.e.* $E_2 < 0$. The critical amplitude for the metastable field lines to exceed the potential barrier (r_{max} for the $E = E_1$ state, the dashed line in figure 7.b) varies with the starting radius, r_0 , but for this profile the critical amplitude is small especially near $r_0 = 0.69$. This means that only a small perturbation is required for the filament to reach the lower energy $E = E_2$ displaced state. In Figure 8, we take a lower value of maximum pressure, however the region where there are third category

Nonlinear ballooning 16

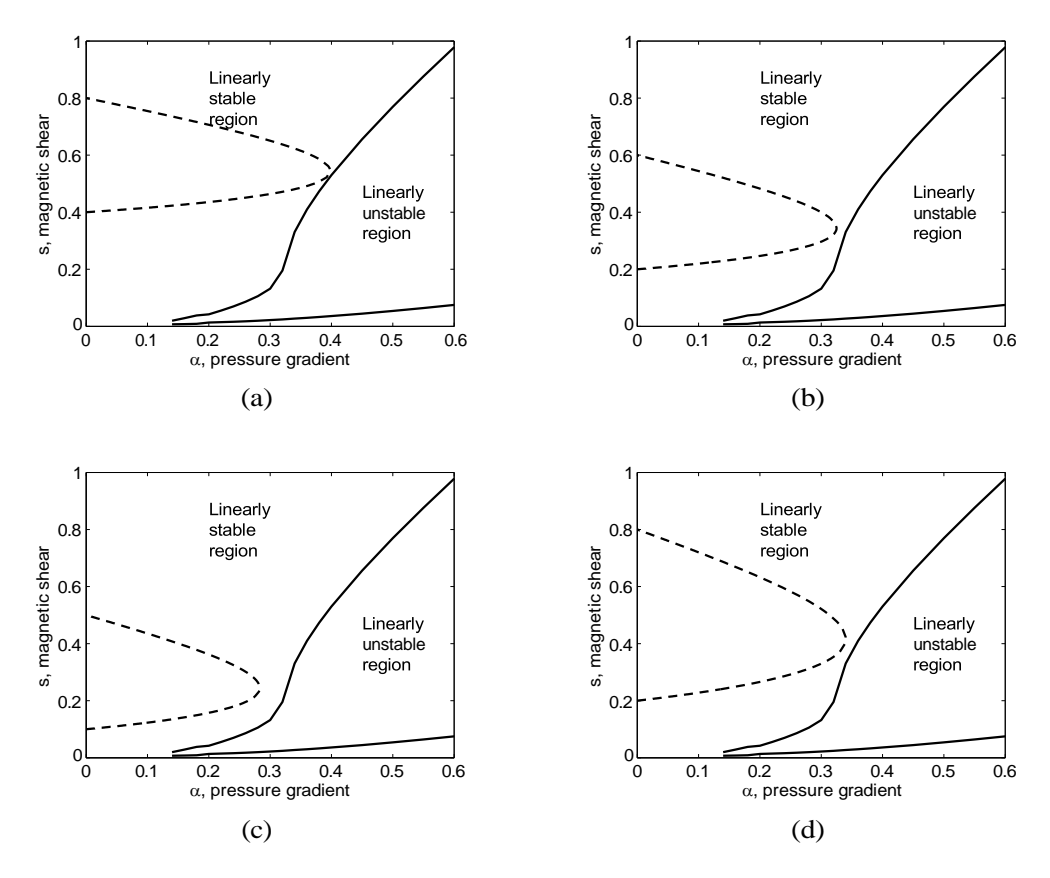


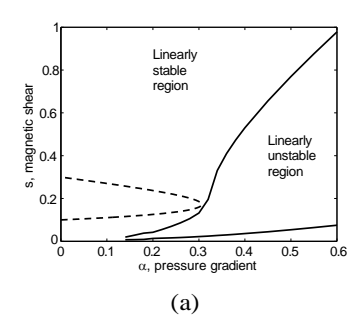
Figure 6: As for Figure 5. The values of shear profiles for each plot are: (a) $s_0 = 0.4$, $s_1 = 0.8$; (b) $s_0 = 0.2$, $s_1 = 0.6$; (c) $s_0 = 0.1$, $s_1 = 0.5$; and (d) $s_0 = 0.2$, $s_1 = 0.8$.

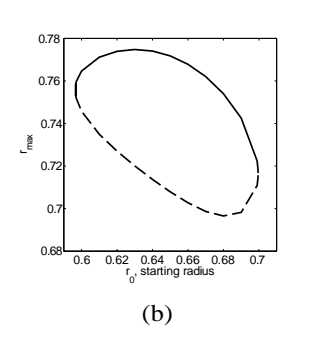
(metastable) field lines is similar $r_0 = 0.65 - 0.69$ to the case in Figure 7. The critical perturbation to reach the lower energy states is larger and the energy released is slightly lower. Finally, Figure 9 uses a yet lower value of α_0 . Here the displacement r_{max} values are similar to the previous cases but the range of r_0 where a displaced states exist is smaller $r_0 = 0.62 - 0.68$ and all these field lines are second category – there is no metastability in this profile.

Note that in these calculations there is a region where lower flux tubes end up in saturated states further out than flux tubes starting further up, i.e. for two flux tubes where $r_{0.1} < r_{0.2}$, we have $r_{max,1} > r_{max,2}$, i.e. the flux tubes overtake.

5.5. Linearly unstable profile

Figure 10 shows a case where the profile crosses the marginal linear stability boundary. For $r_0 = 0.54$ to $r_0 = 0.72$ displaced equilibrium states exist. From $r_0 = 0.54$ to $r_0 = 0.63$ the field lines are in the second category; from $r_0 = 0.63$ to $r_0 = 0.67$ the field lines are in the third category; from $r_0 = 0.67$ to $r_0 = 0.72$ the field lines are in the fourth category (the unperturbed state is linearly unstable); from $r_0 = 0.72$ to $r_0 = 0.723$ the field lines are in the third category but both displaced states have $r_{max} < r_0$ (i.e.





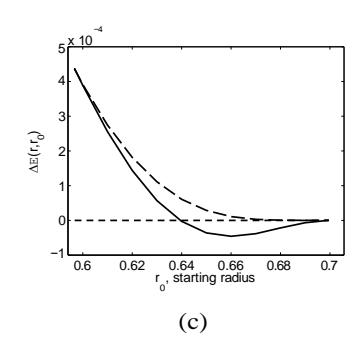
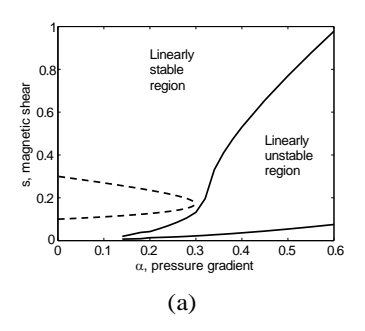
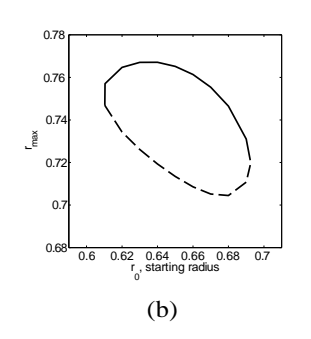


Figure 7: Plot of: (a) trajectory (dashed-dotted line) of the profile in ' $s - \alpha$ ' space; (b) plot of the location of the maximum $r_{max} = r_{eq}(0, r_0)$ of the displaced states (solid line is the E = E₂ state and the dashed line is the E = E₁ state) against starting flux surface r_0 ; (c) the energy change of the displaced states versus the initial position (again solid line is E = E₂ and the dashed line is E = E₁). Here the trajectory approaches the linear ballooning boundary. The region of third category metastable field lines is for starting locations from $r_0 = 0.64$ to $r_0 = 0.7$.





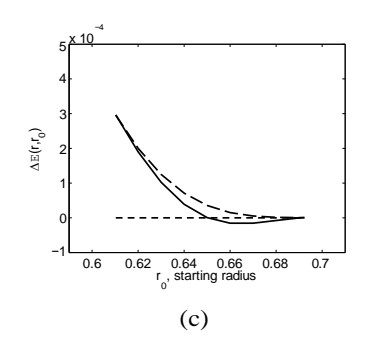
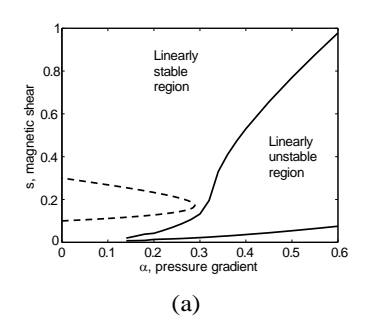
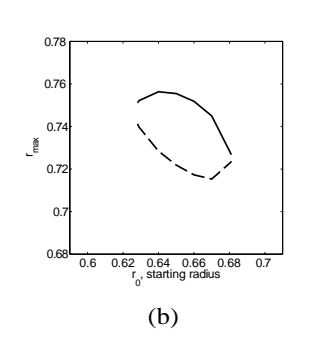


Figure 8: Plot of: (a) trajectory (dashed-dotted line) of the profile in ' $s - \alpha$ ' space; (b) plot of the location of the maximum $r_{eq}(0, r_0)$ of the displaced states (solid line is the $E = E_2$ state and the dashed line is the $E = E_1$ state) against starting flux surface r_0 ; (c) the energy change of the displaced states versus the initial position (again solid line is $E = E_2$ and the dashed line is $E = E_1$). Here the trajectory is further from the linear ballooning boundary than figure (7). The region of third category (metastable) field lines is for starting radii from $r_0 = 0.65$ to $r_0 = 0.69$.

they are displaced inwards) and; from $r_0 = 0.723$ to $r_0 = 0.724$ field lines are in the second category but both displaced states have $r_{max} < r_0$. We see that in the region where the profile is linearly unstable there is no critical perturbation required to access a displaced state and one state, $E = E_2$, is displaced outwards and the other, $E = E_1$, is displaced inwards. The energy change of the outward displaced state $-E_2$ is significantly higher (by several orders of magnitude) than the energy $-E_1$ of the one that is displaced inwards, although both have a lower energy level than the initial state.





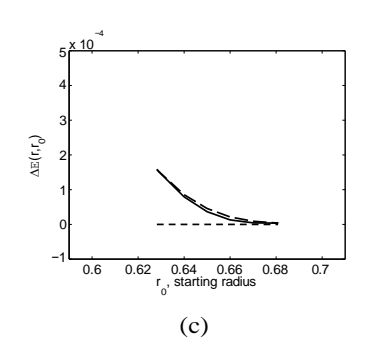
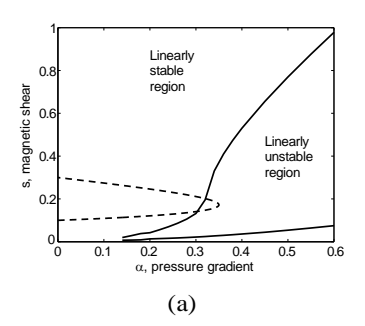
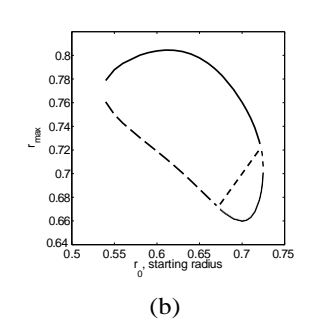


Figure 9: Plot of: (a) trajectory (dashed-dotted line) of the profile in ' $s - \alpha$ ' space; (b) plot of the location of the maximum $r_{max} = r_{eq}(0, r_0)$ of the displaced states (the upper solid line is the $E = E_2$ state and the lower dashed line is the $E = E_1$ state) against starting flux surface r_0 ; (c) the energy change of the displaced states versus the initial position (again solid line is $E = E_2$ and the dashed line is $E = E_1$). Here the trajectory is further still from the linear ballooning boundary. There is no region where the displaced states have lower energy -i.e. all field lines from $r_0 = 0.62$ to $r_0 = 0.68$ are in the second category.





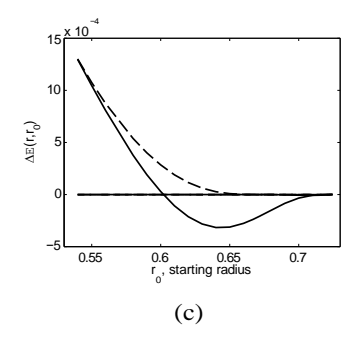


Figure 10: Plot of: (a) trajectory (dashed-dotted line) of the profile in ' $s - \alpha$ ' space. The trajectory crosses the linear ballooning boundary and therefore part of the plasma is linearly unstable. (b) plot of the location of the maximum $r_{max} = r_{eq}(0, r_0)$ of the displaced states (the lower line is the $E = E_2$ state and the upper line is the $E = E_1$ state) against starting flux surface r_0 . The dotted line shows $r_{max} = r_0$. Field lines are in the second category from $r_0 = 0.54$ to $r_0 = 0.63$ and the third category from $r_0 = 0.63$ to $r_0 = 0.67$. From $r_0 = 0.67$ to $r_0 = 0.72$ the unperturbed state is linearly unstable (the fourth category) and one displaced state has $r_{max} > r_0$ and the other displaced state has $r_{max} < r_0$; (c) the energy change of the displaced states versus the initial position (lower line is $E = E_2$ and the upper line is $E = E_1$). From $r_0 = 0.67$ to $r_0 = 0.72$ both displaced states have negative energy $0 > E_1$, E_2 – this is shown by making both lines solid. From $r_0 = 0.72$ to $r_0 = 0.723$ both displacements are inward and field lines are in the third category. From $r_0 = 0.723$ to $r_0 = 0.724$ field lines are in the second category.

6. Discussion and Conclusions

6.1. Discussion

There is ample evidence of filament states in experiments, for example ELM filaments [4] are ubiquitous in tokamak H-mode plasmas and in [14] we discussed the results of Fredrickson [5] where a ballooning mode is responsible for the disruption of an internal transport barrier. More recently core plasma limits have been observed at LHD [6]. These may be driven by a three dimensional version of the phenomena presented here. KSTAR [24] has looked at ELM filament dynamics in more detail experimentally using an ECEI diagnostic. That work shows the emergence of filament structures at the edge of the plasma that saturate and persist for a period of time before the final ELM crash occurs. This at least has qualitative similarity to the saturation phase of the model presented here. We hope to investigate these experimental cases more quantitatively in future work.

It has been suggested [25] that pressure profiles in edge transport barriers (pedestals) are limited by some soft limit from the kinetic ballooning mode (KBM). If this is the case then the profile will sit near the linear ballooning stability boundary. Clearly, in this scenario, the kinetic ballooning modes are assumed to have no explosive behaviour – no access to finitely displaced equilibrium states. However such profiles do develop filamentary eruptions – perhaps when sufficiently large filaments (perhaps arising from low n number instabilities associated with the peeling modes) become unstable. The EPED model [25] predicts that a broad region of the profile should be at the marginal stability boundary. This qualitatively agrees with observed ELMing profiles. The analysis in this paper shows that profiles with a broad region close to the linear stability boundary can have finitely displaced filament equilibria. In future work we will calculate displaced equilibrium states in pedestals with experimental profiles to determine when and how such profiles exhibit explosive instability – ELMs.

Numerical simulations have investigated the eruption of flux tubes, for example [27, 28] where a nonlinear plasma model examined a 2/1 mode in a hybrid scenario and demonstrated that explosive filament growth was possible. Myers *et al* [29] used an ideal MHD model to look at a slab version of the model presented here. They found a time where the simulation first settled down to the linear eigenmode shape, then a linear growth phase followed by a nonlinear growth, and finally an explosive final phase. It is likely that the explosive phase was under resolved and an extended physics model would almost certainly be necessary in this phase.

The two key approximations of the present model are: the unperturbed equilibrium is large aspect ratio and the filaments have an elliptical shape. The large aspect ratio approximation can be relaxed and the metric quantities in Equation (18) can instead be taken from a numerical equilibrium code. Indeed this work is underway. The assumption of the elliptical filaments is more fundamental it is justified by the linear [1] and weakly nonlinear calculations of the expected structure [7, 8] and by the results from numerical investigations [26–29]. The elliptical shape can also be justified from physical intuition.

It is energetically favourable for the erupting flux tube to perturb the ambient external field as little as possible and this is achieved with an elliptic flux tube – this is discussed in Appendix A.

20

Full nonlinear simulations of the process described in this paper are challenging. [27,28] The spatial resolution required to capture for an isolated flux tube is made harder by the discontinuities (current sheets and contact discontinuities) that develop between the tube and its surroundings [10, 26, 29]. Also the temporal resolution requirements to resolve the slow unperturbed equilibrium evolution and the rapid motion of the flux tube are demanding. Nonetheless full understanding of the eruption must surely require extensive numerical investigation.

If we accept that the saturated filament states exist, then it will be important to understand the next steps in the dynamics. It may be that the field lines in the flux tube reconnect with the ambient magnetic field at some location, but it is not obvious where this location is. It maybe that there is significant cross field transport out of the ballooned filament, given there will be a strong temperature gradient as suggested in the 'Leaky hosepipe' model [30]. These issues will be addressed in future work.

6.2. Conclusions

The results shown here exhibit a rich dynamics. The key result is that linearly stable flux tubes can erupt to saturated ballooning states, i.e. they are metastable. The experimental transport barrier profiles are likely to sit near the ballooning mode marginal stability boundary and so these modes are likely to appear if a critical perturbation is available. We conjecture that *hard* stability limits arise when the plasma is in a metastable state with a large energy difference between the unperturbed and perturbed equilibria. The closer the profile is to marginal stability, the larger the region of the plasma that has saturated states available and the more favourable the energy change associated with the saturated states. The current model uses a large aspect ratio ' $s - \alpha$ ' model equilibrium but we fully expect that the key qualitative results will also appear when we use realistic experimental geometry in future work. The model may be able to explain key elements of ITB distruption and ELM dynamics when applied to realistic geometry.

Acknowledgements

The authors would like to thank J W Connor and S Pamela for useful discussions. This work has been carried out within the framework of the EUROfusion Consortium and has received funding from the Euratom research and training programme 2014-2018 under grant agreement No 633053 and from the RCUK Energy Programme [grant number EP/P012450/1]. To obtain further information on the data and models underlying this paper please contact PublicationsManager@ukaea.uk. The views and opinions expressed herein do not necessarily reflect those of the European Commission.

Appendix A. Perturbation of the field outside the filament.

In this paper we have assumed that the perturbations of the field outside the filament have a negligible effect on the filament. Here we estimate the effect of such perturbations. From Fig. 2 the perturbation of the field outside the filament $\delta B_{\text{out}} \sim B_0(\frac{\delta 1}{2}) \hat{n}$ $B_0(\frac{\delta_1}{\delta_2})\sin\theta$ $\hat{\mathbf{n}}$ where $\hat{\mathbf{n}} = \nabla S/|\nabla S|$ and $B_0 \cdot B_{in} = B_0 B_{in} \cos\theta$. Thus the curvature

force on one side of the filament in the
$$\nabla S$$
 direction is
$$\frac{1}{\mu_0} (B_{\text{out}} \cdot \nabla B_{\text{out}}) \cdot \hat{\mathbf{n}} \sim \frac{1}{\mu_0} B^2 \frac{\delta_1}{\delta_2^2} \sin^2 \theta. \tag{A.1}$$

For a symmetric filament the net force from the external curvature forces on the two sides cancel. A shift of the filament by a distance of order δ_1 in the $\hat{\mathbf{n}}$ direction changes the curvature forces by a factor of order one. Thus an asymmetric filament can adjust its position by a negligible shift to achieve net force balance. However the curvature forces squeeze the filament from both sides and change the pressure balance. Thus there is a perturbation of the total internal pressure:

$$\delta(\mu_0 p_{in} + \frac{B^2}{2}) \sim B_0^2 \frac{\delta_{\underline{l}}^2}{\delta_2^2} \sin^2 \theta.$$
 (A.2)

This pressure perturbation varies finitely in the filament – it will try to elongate (flatten)

the filament in the
$$e_{\perp}$$
 direction. The extra elongating force in the e_{\perp} direction is
$$\delta \mathbf{F} \cdot \mathbf{e}_{\perp} = \delta F_{\perp} \sim \frac{1}{\mu_0} \frac{\delta(\mu p_{\perp} + \frac{B^2}{2})}{r\delta_2} \sim \frac{1}{\mu_0} B_0^2 \frac{\delta_1^2}{r\delta_2^3} \sin^2 \theta. \tag{A.3}$$

Note that $\sin \theta \sim \frac{\Delta r}{\sigma R_0}$ where Δr is the radial displacement of the filament. Estimating the force on a perturbed filament ignoring the external perturbations we get:

$$F_{\perp} \sim \frac{B_0^2}{\mu_0 q R_0^2 r} \Delta r \sim \frac{B_0^2}{\mu_0 R_0 r} \sin \theta \tag{A.4}$$

Thus the external perturbations can be ignored if:

$$\delta F_{\perp} \ll F_{\perp} \to \frac{\delta_1^2 R_0}{\delta_2^3} \sin \theta \ll 1.$$
 (A.5)

This provides a condition on the ellipticity of the filament for our treatment to be correct. In linear theory, [1], the eigenfunction across the field is elongated $(\delta_1 \sim \frac{R0}{n}, \delta_2 \sim \frac{R0}{n})$ with $n \gg 1$) – thus in this case $\delta F_{\perp} \sim n^{-1/2} \sin \theta F_{\perp} \ll F_{\perp}$. In the weakly nonlinear theory [7, 8, 12, 13] the linear eigenfunction evolves into an even narrower elliptical flux tube. The weakly nonlinear theory includes the external perturbations and the interaction of filaments because the displacement is ordered to be small $\Delta r \sim \delta_1 \sim \frac{R0}{2}$ and the system is assumed to be close to marginal stability so that $\delta F_{\perp} \sim F_{\perp}$. However as the filaments evolve in the weakly nonlinear theory they evolve into the isolated tubes considered here [11, 13].

As shown above elliptical tubes that originate as perturbations of the linear eigenfunction shape are expected to be unaffected by the perturbation of the external field. The external forces will, however, often change the shape of the filament -

specifically flattening the ellipse – detailed calculation of this flattening is beyond the scope of this paper. Nonetheless we can estimate the flattening of the displaced equilibrium filament. To lowest order the displaced equilibrium field lines satisfy $F_{\perp}(r, \theta, r_0) = 0$ giving $r = r_{sat}(\theta, r_0)$ – solutions of equations (17), (6) and (12). For small displacements about this lowest order solutions we can write $r = \delta r(\theta, r_0) + r_{sat}(\theta, r_0)$ and linearise the force operator $F_{\perp} \sim L_{sat}(\delta r)$. Thus equilibrium is modified

$$\delta F_{\perp} + F_{\perp} \sim \delta F_{\perp} + L_{sat}(\delta r) = 0.$$
 (A.6)

Estimating δr we obtain:

$$\frac{\delta r}{qR_0} \sim \frac{\delta_1^2 R_0}{\delta_2^3} \sin^2 \theta. \tag{A.7}$$

For the linear eigenfunction shape $\delta r \sim \delta_2 \sin^2 \theta$. Thus when the displacement is finite $(\sin \theta \sim 1)$ the filament is flattened by order the elongation *i.e.* $r = r_{sat} + O(\delta_2)$. This is a finite change in the shape but a small change in the filament position. We hope to develop a asymptotic solution of the equilibrium shape in future work.

We have focussed on perturbations shaped like the linear eigenfunctions since these will be easier to destabilise (even in metastable situations). It is possible that in some meta-stable cases a finite perturbation with a shape that violates the condition in equation (A.5) can be destabilised. We cannot treat such cases with the method developed in this paper.

Appendix B. Model equilibrium

In these notes we calculate the large aspect ratio $(q = r/R \ll 1)$ equilibrium with two regions; an *Outer Region* where the pressure gradient is small $(rp'/B^2 \sim O(q^2))$ and a narrow $(\Delta r \sim qr)$ *Transport Barrier* around r = rT B where the pressure gradient is close to the ballooning threshold $(rp'/B^2 \sim O(q))$. Note that the plasma beta is everywhere small i.e. $p/B^2 \sim O(q^2)$. We shall take the safety factor, q, and the global magnetic shear, rq', to be finite in the transport barrier – however r^2q'' can be large in the transport barrier. All symbols have their usual meaning!

Appendix B.1. Inverse Equilibrium

We use the usual inverse equilibrium approach of Weimer, Greene and Johnson. The radial variable r labels flux surfaces, θ is a poloidal angle and φ is the usual cylindrical toroidal angle. In axisymmetry the cylindrical coordinates (R, φ, Z) are functions of the flux coordinates $(r, \theta) - i.e.$ $R = R(r, \theta)$ and $Z = Z(r, \theta)$.

The magnetic field is given by:

$$B = \bar{B}_0 R_0 \{ f(r) \nabla \varphi \times \nabla r + g(r) \nabla \varphi \}$$
(B.1)

where \vec{B}_0 is a normalising field so that $g \sim O(1)$ and R_0 is the radius of the magnetic axis. The equilibrium Grad-Shafranov equation in flux coordinates is:

$$\frac{1}{r}\frac{\partial}{\partial r}(rf|\nabla r|^{2}) + f\frac{\partial}{\partial \theta}(\nabla r \cdot \nabla \theta) + \frac{1}{f}(gg' + \frac{R^{2}}{R_{0}^{2}B_{0}^{2}}p') = 0.$$
(B.2)

The jacobian of the transformation to the flux coordinates (r, θ, φ) is chosen to keep the field lines *straight* in $\theta - \varphi$ space on a flux surface:

$$\mathbf{J} = (\nabla r \times \nabla \theta \cdot \nabla \varphi)^{-1} = \frac{rR^2}{R_0} = R \frac{\left(\frac{\partial R}{\partial \theta} \frac{\partial Z}{\partial r} - \frac{\partial R}{\partial r} \frac{\partial Z}{\partial \theta}\right)}{\left(\frac{\partial R}{\partial r} \frac{\partial Z}{\partial r} - \frac{\partial R}{\partial \theta}\right)}$$
(B.3)

and then the safety factor is $q(r) = \frac{rg}{Ror}$. Note that:

$$(\nabla r \times \nabla \theta) = \frac{R_0}{r} \nabla \varphi \tag{B.4}$$

We expand R and Z as:

$$R = R_0 + r\cos\theta + \tilde{R}_1(r)\cos 2\theta + \bar{R}_1(r) + O(\rho^2 r)....$$

$$Z = -r\sin\theta + \tilde{Z}_1(r)\sin 2\theta + O(\rho^2 r).....$$
(B.5)

where \tilde{R}_1 , \bar{R}_1 and \tilde{Z}_1 are O(qr). We have chosen $\theta = 0$ to be the outer (larger R) mid-plane of each flux surface – this differs from the choice in [16] where $\theta = 0$ is on the inner R mid-plane. We define \vec{B}_0 so that:

$$g = 1 + g_2 + O(q^3), \quad g_2 \sim O(q^2)$$
 (B.6)

and
$$q$$
 is finite so that $f = f_1 = \frac{r}{R_0 q} + O(\varrho^2)$. To denote order we write $p(r) = p_2(r)$.

We seek expanded expressions as functions of r and θ of the metric elements:

$$|\nabla r|^2 = \frac{R_0^2}{r^2 R^2} \frac{i}{\partial \theta} + \frac{\partial Z}{\partial \theta} \frac{i}{\partial \theta} + \frac{\partial Z}{\partial \theta} \frac{i}{\partial \theta} \frac{i}{r^2 R^2} \frac{\partial R}{\partial \theta} \frac{\partial R}{\partial \theta} \frac{\partial R}{\partial r} \frac{\partial Z}{\partial \theta} \frac{\partial Z}{$$

to substitute into the ballooning equations of Section 2.

The regions are:

Outer Region where $|r - r_{TB}| \gg qr$ and all radial derivatives are finite *i.e.*

$$\frac{\partial}{\partial r} \sim O(\frac{1}{r}), \quad \frac{\partial \tilde{R}_1}{\partial r}, \quad \frac{\partial \tilde{Z}_1}{\partial r}, \quad \frac{\partial \tilde{R}_1}{\partial r} \sim O(\varrho),$$

$$rp'/B^2 \sim O(\varrho^2), \quad rg' \sim O(\varrho^2) \quad and \quad f, rf' \sim O(\varrho)$$
(B.8)

Transport Barrier where $|r - r_{TB}| \sim \rho r$ and radial derivatives are large:

$$\frac{\partial}{\partial r} \sim O(\frac{1}{\varrho r}), \quad \frac{\partial \tilde{R}_1}{\partial r}, \quad \frac{\partial \tilde{Z}_1}{\partial r}, \quad \frac{\partial \bar{R}_1}{\partial r} \sim O(\frac{1}{\varrho}),$$
 (B.9)

$$rp'/B_{0}^{2} \sim O(q)$$
, $rg'_{2} \sim O(q)$ and $f, rf' \sim O(q)$ but $r^{2}f'', r^{2}g'' \sim O(1)$

Appendix B.2. Outer Region

Substituting expressions from Eq. (B.5) into Eq. (B.3) we obtain:

$$\frac{r^{2} \cos \theta}{R_{0}} = 2R_{1} \sin \theta \sin 2\theta - 2Z_{1} \cos \theta \cos 2\theta - r \sin \theta \sin 2\theta \frac{\partial \tilde{Z}_{1}}{\partial r} + r \cos \theta \cos 2\theta \frac{\partial \tilde{R}_{1}}{\partial r} + r \cos \theta \frac{\partial \tilde{R}_{1}}{\partial r} + O(r q^{2})$$
(B.10)

which yields:

$$\tilde{Z}_1 = -\tilde{R}_1$$

$$r\frac{\partial \bar{R}_{1}}{\partial r} = \frac{r^{2}}{R_{0}} - 2\tilde{R}_{1} - r\frac{\partial \tilde{R}_{1}}{\partial r}$$
(B.11)

From Eq. (B.7) we define Δ' so that:

$$|\nabla r|^2 = 1 + 2\Delta' \cos \theta \dots$$

and

$$\nabla r \cdot \nabla \theta = -\frac{1}{r} r \Delta'' + \Delta' + \frac{r}{R_0} \sin \theta.$$
 (B.13)

We will need:

$$\frac{R^2}{R_0^2} = 1 + \frac{2r}{R_0}\cos\theta - \frac{(r^2 + \frac{2\Delta}{R_0} + \frac{r\Delta'}{R_0} + \frac{r\Delta'}{R_0} + \frac{3r^2}{2R_0^2}\cos 2\theta. \quad (B.14)$$

and

$$|\nabla \theta|^2 = \frac{1}{r^2} (\frac{r}{1 + 2(\frac{r}{R_0} - \Delta')\cos\theta + (r\Delta''\sin\theta)^2....O(\varrho^2)})$$
(B.15)

We have kept the terms that become large in the transport barrier – where $r\Delta'' \sim 1$. The equilibrium relation, Eq. (B.2), becomes to $O(q^2)$:

$$\frac{1}{r}\frac{d}{dr}(rf_1) + \frac{1}{f_1}g_2' + \frac{p_2'}{I_0^2} = 0$$
(B.16)

$$\Delta'' = \frac{1}{R_0} - \frac{2R_0q^2}{r} \frac{\dot{p}_2}{\bar{l}_0^2} - \frac{3}{r} - 2\frac{2}{q} \frac{dq}{dr} \Delta'$$
(B.17)

Appendix B.3. Transport barrier

The equations derived in the previous section, Eqs. (B.12) - (B.17), remain valid to the order we need. Since q and r are roughly constant across the Transport barrier we can integrate Eq. (B.16) for $g_2^{'}$ and Eq. (B.17) for $\Delta^{'}$ in the layer.

$$g_2 = -\frac{p_2}{\bar{I}_0^2} + constant \tag{B.18}$$

$$\Delta'' \sim -\frac{2R_0q^2}{r} \frac{p_2'}{\bar{I}_0^2} \sim O(\frac{1}{r}) \rightarrow \Delta' = -\frac{2R_0q^2}{r} \frac{p_2}{\bar{I}_0^2} + constant$$
(B.19)

Note the constants are slowly varying functions of r so they are effectively constant across the transport barrier. The magnetic shear is taken to be finite and finitely varying across the barrier, so that:

$$f_{1} = f(r) + f(\frac{r - r_{0}}{r})$$

$$q' = \frac{d}{dr} \frac{R_{0}f_{1}}{r} + \frac{R_{0}f_{2}}{r} \dots$$
(B.20)

We introduce the s and α parameters of Connor, Hastie, Taylor [1]:

$$s = \frac{rq}{q}$$

$$\alpha = -2R \frac{q^2}{\sqrt{\frac{r_2}{\Gamma_0^2}}}$$
(B.21)

Note that both these parameters are finite and vary finitely over the transport barrier so that $s' \sim O(\frac{1}{\rho})$ and $\alpha' \sim O(\frac{1}{\rho})$. Then $\Delta'' = \alpha$. To lowest (finite) order the metric coefficients are

$$|\nabla r|^{2} = 1$$

$$\nabla r \cdot \nabla \theta = \frac{2R_{0}q^{2} p_{2}^{'}}{r l_{0}^{2}} \sin \theta = -\frac{\alpha}{r} \sin \theta \qquad (B.22)$$

$$|\nabla \theta|^{2} = \frac{1}{r^{2}} 1 + (2R q^{2} \frac{p_{2}^{'}}{l_{0}^{2}} \sin \theta)^{2} O(q) = \frac{1}{r^{2}} [1 + (\alpha \sin \theta)^{2} O(q)]$$

We shall also need the derivatives of R.

$$\frac{\partial R}{\partial r} = \cos \theta - \alpha \sin^2 \theta + O(\varrho)....$$

$$\frac{\partial R}{\partial \theta} = -r \sin \theta + O(\varrho)....$$
(B.23)

Appendix C. Weak Nonlinearity - with Inertia

Here we investigate the weakly nonlinear case with inertia. The dynamics is interesting because the mode spreads along the field lines as it evolves explosively. With inertia

and $r - r_0 \sim qr$ equation (32) becomes:

$$\tau_A \frac{\partial^2 r}{\partial t^2} \left[1 + (\alpha \sin \theta - s\theta)^2 \right] =$$

 $(\beta_N(r_0) - \beta_N(r)) [\cos \theta + \sin \theta (s\theta - \alpha \sin \theta)]$

$$+\frac{\partial}{\partial \theta} \left[1 + (\alpha \sin \theta - s\theta)^{2}\right] \frac{\partial r}{\partial \theta} - \frac{1}{2} \frac{\partial r}{\partial \theta} \frac{\partial r}{\partial \theta} - \frac{1}{2} \frac{\partial r}{\partial \theta} \frac{\partial r}{\partial \theta} \frac{\partial r}{\partial \theta} \frac{\partial r}{\partial \theta} + \frac{1}{2} \frac{\partial r}{\partial \theta} \frac{\partial r}{\partial \theta$$

where $\tau_A^2 = \frac{\mu^0 \rho o q^2 R_0^2}{B_0^2}$. If $x = r - r_0 \sim O(\delta r) \ll \rho r$ and we are close to marginal stability $\tau_A^2 \frac{\partial^2 x}{\partial t^2} \sim O(\frac{\delta^2 x}{\rho^2})$, Eq. (C.1) can be expanded in powers of x. We define the linear

$$L(x) = \alpha_0 \left[\cos \theta + \sin \theta (s_0 \theta - \alpha_0 \sin \theta)\right] x$$

$$+ \left(\frac{\partial}{\partial \theta}\right) \left[1 + (\alpha \sin \theta - s \theta)^2\right] \left(\frac{\partial x}{\partial \theta}\right) - \frac{\partial \theta}{\partial \theta}$$

$$(C.2)$$

where
$$s_0 = s(r_0)$$
 and $\alpha_0 = \alpha(r_0)$. The expanded nonlinear operator is:
$$N(x, x) = \frac{\alpha'_0}{2} \cos \theta + \theta \sin \theta (\frac{\alpha'_0 s_0}{2} + s'_0 \alpha_0) + \frac{3\alpha'_0 \alpha_0}{2} \sin^2 \theta x^2$$

$$+ \frac{\partial}{\partial \theta} \sum_{r_0} (\alpha'_0 \sin \theta - s'_0 \theta)(\alpha_0 \sin \theta - s_0 \theta) x \frac{\partial x}{\partial \theta} \sum_{r_0} (\alpha'_0 \sin \theta - s'_0 \theta)(\alpha_0 \sin \theta - s_0 \theta)$$
(C.3)

and $s_0' = \frac{ds_0}{dr_0} \sim \frac{1}{\rho r}$ and $\alpha_0' = \frac{d\alpha_0}{dr_0} \sim \frac{1}{\rho r}$. The equation of motion, to the order we need becomes

$$\tau_A^2 \left(\frac{\partial^2 x}{\partial t^2} \right) \left[1 + (\alpha \sin \theta - s\theta)^2 \right] = L(x) + N(x, x)$$
 (C.4)

The solution has two regions: an inner region where $\theta \sim 0(1)$ and inertia is unimportant and an outer region where $\theta \sim O(\rho/\delta)$ and nonlinearity is unimportant. This is similar to the treatment in [8].

Appendix C.1. Inner region

In the region $x \sim O(\delta)$ the left hand side of Eq. (C.4) (inertia) is $\sim O(\delta^3/\rho^2)$. The nonlinear term is of order $\sim O(\delta^2/\varrho)$. To order δ we have:

$$0 = L(x) + O(\delta^2)$$
 (C.5)

Then we can write:

$$x(\theta, t) = A(t)xL(\theta) + \delta x(\theta, t)$$
 (C.6)

where $x_L(\theta)$ is the linear solution to $L(x_L) = 0$ that is even in θ and normalised so that $x_L(0) = 1$ – thus $A \sim O(\delta)$. $\delta x(\theta, t) \sim O(\delta^2/\varrho)$ is driven by the nonlinear term. As we

will see below, the solution as
$$|\theta| \to \infty$$
 consists of the "small" and "large" solutions:

$$x_L(\theta) \to x_{LL} + \frac{x_{SL}}{\theta} = x_{SL} \cdot \frac{1}{\theta} + \frac{1}{\Delta}$$
(C.7)

where x_{SL} x_{LL} and $\Delta = x_{SL}/x_{SL}$ are constants. To be consistent we need to be sufficiently close to marginal stability $(\frac{1}{\sqrt{1}} = 0)$ such that $\frac{1}{\sqrt{1}} \sim O(\delta/\varrho)$. Thus the "large" solution is the same size as $\delta x(\theta, t) \sim O(\delta^2/\rho)$ and we must calculate the corrections due to the nonlinear term to get the correct asymptotic behaviour when $\theta \gg 1$. To order $O(\delta^2/\rho)$ the inner region solution satisfies:

$$0 = L(x) + A^{2}N(x_{L}, x_{L})$$
 (C.8)

Multiplying Eq. (C.8) by $x_L(\theta)$ and integrating from $\theta = 0$ to $\theta = \theta_m$ (in the matching region where $1 \ll \theta_m \ll \rho/\delta$) we obtain:

The constant c_{NL} defined by Eq. (C.9) is O(1) and insensitive to the choice of θ_m as long as it is in the range $1 \ll \rho / \delta$ – the particular choice makes a difference to c_{NL} of order δ^2/ρ^2 . Since the nonlinear terms in Eq. (C.8) die away rapidly for asymptotically large θ (see next subsection) we can write: $x(\theta) \to A(t) \frac{x_{SL}}{\theta} + x_{Large}(t)$

$$x(\theta_{m}) \to A(t)^{\frac{\chi_{SL}}{H}} + x_{Large}(t)$$
(C.10)

Substituting into Eq. (C.9) we obtain the relation

$$-\frac{x_{Large}(t)}{x_{SL}} = -\frac{A}{\Delta'} + c'_{NL}A^2. \tag{C.11}$$

where $c'_{NL} = \frac{c_{NL}}{s^2 \chi^2}$.

Appendix C.2. Outer Solution

Now let us expand Eq. (C.4) in powers of δ with $\frac{\partial}{\partial t} \sim O(\delta/\varrho)$, $\theta \sim O(\varrho/\delta)$ and $x \sim O(\delta^2/q)$. We treat the θ variation as having two scales: the fast periodic scale $\frac{\partial}{\partial \theta_f} \sim O(1)$ and the slow scale $\frac{\partial}{\partial \theta_s} \sim O(\delta/\varrho)$; then $\frac{\partial}{\partial \theta} = \frac{\partial}{\partial \theta_f} + \frac{\partial}{\partial \theta_s}$ and $\theta_s \sim O(\varrho/\delta)$ – thus $x(\theta_f, \theta_s, t)$. We write $x = x_2 + x_3 + x_4$ where $x_n \sim O(\delta^n/\varrho^{n-1})$. To $O(\varrho)$ we obtain:

$$0 = \theta_s^2 \frac{\partial^2 x_2}{\partial \theta_f^2} \rightarrow x_2 = x_2(\theta_s, t)$$
 (C.12)

In $O(\delta)$ we obtain:

$$0 = s_0^2 \theta_s^2 \frac{\partial^2 x_3}{\partial \theta_f^2} + \alpha_0 s_0 \sin \theta_f \theta_s x_2 \rightarrow x_3 = x_2 \frac{\alpha_0 \sin \theta_f}{s_0 \theta_s}$$
 (C.13)

In $O(\delta^2/q)$ we obtain

$$\frac{\partial^{2} \partial x_{1}}{\partial x_{1} \partial x_{2}} = \alpha_{0} \cos \theta_{f} x_{2} + s_{0} \frac{\partial}{\partial \theta_{s}} \theta_{s}^{2} \frac{\partial x_{2}}{\partial \theta_{s}} + \frac{\partial}{\partial \theta_{s}} \frac{\partial^{2} \partial x_{2}}{\partial \theta_{s}} + \frac$$

Note the largest nonlinear term is $O(\delta^3/\rho)$ and is therefore ignored to this order. We average Eq. (C.14) over the fast scale θ_f to obtain the evolution equation for x_2 :

$$\tau_A^2 \theta_s^2 \frac{\partial^2 x_2}{\partial t^2} = \frac{\partial}{\partial \theta_s} \theta_s^2 \frac{\partial x_2}{\partial \theta_s}$$
 (C.15)

Since x_2 only depends on the one, slow, scale we drop the subscript s on θ and write

$$x_2 = \frac{f(\theta, t)}{\theta}$$
. Then Eq. (C.15) becomes the wave equation:

$$\tau_A \frac{\partial^2 f}{\partial t^2} = \frac{\partial^2 f}{\partial \theta^2}$$
(C.16)

To satisfy the boundary conditions we take outgoing waves:

$$f(\theta, t) = f(t - \tau_A \theta). \tag{C.17}$$

Now we match our solution to the inner solution: The outer solution for $1 \ll \theta \ll \rho/\delta$

matches Eq. (C.10), so expanding
$$x_2$$
 for small θ we find:
$$x_2 = \frac{f(t - \tau_A \theta)}{\theta} \to \frac{f(t)}{\theta} - \tau_A \frac{df(t)}{dt} = A(t) \frac{x_{SL}}{\theta} + x_{Large}(t) \tag{C.18}$$

Thus:

$$f(t) = A(t)xsL$$
 and $x_{Large}(t) = -\tau_A \frac{df(t)}{dt} = -xsL\tau_A \frac{dA}{dt}$ (C.19)

Then Eq. (C.11) becomes:

$$\tau_{A} \frac{dA}{dt} = -\frac{A}{\Delta'} + c'_{NL} A^{2}. \tag{C.20}$$

Note this equation is only valid close to the marginal point where $\Delta' \sim O(\varrho/\delta)$. The solution for $A(t = 0) = A_0$ is:

$$A(t) = A_0 e^{\gamma t} \frac{1}{1 + cA_0(e^{\gamma t} - 1)}$$
 (C.21)

where
$$\tau_{AY} = -\Delta^{'-1}$$
 and $c = c'_{NL}\Delta'$. The potential energy for this system is:

$$V(A) = -\frac{1}{\tau_{AY}} \frac{A^2}{2} - c\frac{A^3}{3}$$
(C.22)

29

For linearly damped modes ($\gamma < 0$) the energy has a local minimum (V = 0) at A = 0and a local maximum $(V = 1/(6c^2\tau_A|\gamma|))$ at A = 1/c. If the initial condition $cA_0 < 1$ then as $t \to \infty$ then $A \to 0$. When $cA_0 > 1$ the solution grows explosively and reaches a finite time singularity when $t = (1/\gamma) \ln (1 - \frac{1}{\epsilon 4n})$ (see [7]). In this case the field line is in the third category see Figure (4.c). Clearly the weak nonlinear assumption will be violated before the tube reaches infinite amplitude – a full nonlinear solution is needed in these cases to find the final equilibrium with energy E_2 . When $\gamma > 0$ the field line is in the fourth category see Figure (4.d) but again the lowest energy equilibrium state is outside the amplitude expansion. In [7] and [8] the weak nonlinear dynamics close to linear marginal stability is treated without the assumption of isolated flux tubes – this is a more complete treatment than this appendix since it includes the evolution of the flux tube cross section. Zhu et. al. [9, 10] have explored an expansion which extends the weakly nonlinear analysis from amplitudes of order δ_1 to amplitudes of order δ_2 . To determine the equilibria the finite amplitude treatment explored in this paper is required.

References

- [1] J. W. Connor, R. J. Hastie and J. B. Taylor, Proc. R. Soc. London A365 (1979)
- [2] J. W. Connor, J. B. Taylor, and M. Turner, Nucl. Fusion 24 642(1984)
- [3] J. W. Connor Plasma Phys. Control. Fusion 40 531 (1998)
- [4] A. Kirk, et. al., Phys. Rev. Lett. 96 185001 (2006)
- [5] E. D. Fredrickson, et. al. *Phys. Plasmas* 3 2620 (1996)
- [6] S. Ohdachi, et al. Nucl. Fusion 57 066042 (2017)
- [7] S. C. Cowley and M. Artun, *Physics Reports*, vol. 283, pp. 185 211, 1997.
- [8] H. R. Wilson and S. C. Cowley, Phys. Rev. Lett., vol. 92, no. 17, 175006-1-175006-4, (2004).
- [9] P. Zhu, C. C. Hegna, C. R. Sovinec, A. Bhattacharjee, and K. Germaschewski, Nucl. Fusion vol. 49, 095009 (2009)
- [10] P. Zhu, C. C. Hegna and, C. R. Sovinec, Phys. Rev. Lett. vol. 102, 235003 (2009)
- [11] S. C. Cowley, B. Cowley, S. A. Henneberg and H. R. Wilson, Proc. R. Soc. A 471 20140913(2015)
- [12] S. A. Henneberg, S. C. Cowley and H. R. Wilson Plasma Phys. Control. Fusion 57 125010 (2015)
- [13] S. A. Henneberg, S. C. Cowley and H. R. Wilson Contributions to Plasma Physics 58 6-20(2018)
- [14] C. J. Ham, S. C. Cowley, G. Brouchard and H. R. Wilson Phys. Rev. Lett. 116 235001 (2016)
- [15] J. W. Connor, R. J. Hastie and J. B. Taylor, Phys. Rev. Lett. 40 396(1978)
- [16] J. M. Greene, J. L. Johnson and K. E. Weimer, Phys. Fluids. 14 671 (1971)
- [17] T.C. Hender, et. al. Nucl. Fusion, 47, S128 S202(2007).
- [18] H. R. Wilson, S. C. Cowley, A. Kirk and P. B. Snyder Plasma Phys. Control. Fusion 48 A71-A84 (2006)
- [19] P. B. Snyder, et. al., Nucl. Fusion, 51, 103016 (2011).
- [20] J. W. Connor, et. al., Phys. Fluids. 31 577(1988)
- [21] F. Troyon, R. Gruber, H. Saurenmann, S. Semenzato and S. Succi, Plasma Phys. Control. Fusion 26 209(1984)
- [22] S. C. Cowley, B. Cowley, S. A. Henneberg and H. R. Wilson, arXiv preprint arXiv:1411.7797 (2014),

- [23] H. R. Struass Phys. Fluids 24 2004 (1981)
- [24] G. S. Yun, et al. Phys. Rev. Lett., vol. 107, 045004, 2011.
- [25] P. B. Snyder, et. al. Nucl. Fusion 51 103016 (2011)
- [26] B. H. Fong. Metastable and explosive properties of ballooning modes in laboratory and space plasmas. PhD thesis, Princeton University. (2000)

30

- [27] A. Y. Aydemir, et al. Nucl. Fusion 56 054001 (2016)
- [28] A. Y. Aydemir, et al. Nucl. Fusion 58 016026 (2018)
- [29] S. A. Myers, et al. Plasma Phys. Control. Fusion 55 125016 (2013)
- [30] H. R. Wilson, et al. Plasma Phys. Control. Fusion 48 A71 (2006)